



True-Stain Monocyte Blocker™
Block Monocyte Non-Specific Antibody Binding



Intracellular BH3 Profiling Reveals Shifts in Antiapoptotic Dependency in Human B Cell Maturation and Mitogen-Stimulated Proliferation

This information is current as of January 25, 2018.

Joanne Dai and Micah A. Luftig

J Immunol published online 22 January 2018
<http://www.jimmunol.org/content/early/2018/01/22/jimmunol.1701473>

Supplementary Material <http://www.jimmunol.org/content/suppl/2018/01/22/jimmunol.1701473.DCSupplemental>

Why *The JI*?

- **Rapid Reviews! 30 days*** from submission to initial decision
- **No Triage!** Every submission reviewed by practicing scientists
- **Speedy Publication!** 4 weeks from acceptance to publication

**average*

Subscription Information about subscribing to *The Journal of Immunology* is online at: <http://jimmunol.org/subscription>

Permissions Submit copyright permission requests at: <http://www.aai.org/About/Publications/JI/copyright.html>

Email Alerts Receive free email-alerts when new articles cite this article. Sign up at: <http://jimmunol.org/alerts>

The Journal of Immunology is published twice each month by The American Association of Immunologists, Inc., 1451 Rockville Pike, Suite 650, Rockville, MD 20852
Copyright © 2018 by The American Association of Immunologists, Inc. All rights reserved.
Print ISSN: 0022-1767 Online ISSN: 1550-6606.



Intracellular BH3 Profiling Reveals Shifts in Antiapoptotic Dependency in Human B Cell Maturation and Mitogen-Stimulated Proliferation

Joanne Dai and Micah A. Luftig

Apoptosis is critical to B cell maturation, but studies of apoptotic regulation in primary human B cells is lacking. In this study, we sought to better understand the mechanisms of apoptotic regulation in normal and activated B cells. Using intracellular BH3 profiling, we defined the Bcl2 dependency of B cell subsets from human peripheral blood and tonsillar lymphoid tissue as well as mitogen-activated B cells. We found that naive and memory B cells were BCL-2-dependent, whereas germinal center B cells were MCL-1-dependent and plasma cells were BCL-X_L-dependent. B cells stimulated to proliferate ex vivo by CpG or CD40L/IL-4 became more dependent on MCL-1 and BCL-X_L. As B cell lymphomas often rely on survival mechanisms derived from normal and activated B cells, these findings offer new insight into potential therapeutic strategies for lymphomas. *The Journal of Immunology*, 2018, 200: 000–000.

The maturation of B cells into Ab-secreting cells is critical to immunity and is accomplished through either T-independent or T-dependent B cell maturation. In T-independent B cell maturation, Ag binding to the BCR stimulates extrafollicular naive and memory B cells to proliferate (1). B cells can also be activated via pathogen-associated molecular patterns, such as CpG DNA, binding to TLR (2, 3). Activated B cells can differentiate into short-lived plasmablasts or migrate into secondary lymphoid tissue to undergo T-dependent maturation. In the germinal center (GC) reaction, the affinity for Ag is further refined through somatic hypermutation and selection by apoptosis (4). B cells also compete for survival signals in the form of Ag binding to the BCR and CD40 receptor binding to cognate T follicular helper cells. Outcompeted B cells are eliminated by apoptosis, and surviving B cells exit the GC as long-lived memory B cells or plasma cells.

Ultimately, the humoral repertoire is shaped by apoptosis dependent on the multidomain Bcl-2 family proteins that select which B cells die and which continue to propagate (5). The Bcl-2 family is subdivided into three structural and functional classes: the

prosurvival Bcl-2 family members (BCL-2, BCL-X_L, BCL-W, MCL-1, and BFL-1), the BH3-only proapoptotic proteins (BAD, BID, BIM, BMF, BIK, HRK, NOXA, and PUMA), and the proapoptotic multidomain family members (BAK, BAX, and possibly BOK). Apoptosis is initiated when BAX and BAK homooligomerize to form higher molecular mass structures that facilitate mitochondrial outer membrane permeabilization to release cytochrome *c* and proapoptogenic factors into the cytosol, which activate a cascade of caspases that mediate DNA fragmentation, protein degradation, and cellular blebbing (6). To prevent aberrant activation, antiapoptotic proteins bind and sequester BAX and BAK as well as the proapoptotic BH3-only proteins (named as such because they share homology in their BH3 domain). Dysregulation of apoptosis typically accompanies the development of lymphomas or autoimmunity, and understanding the mechanisms of apoptosis regulation is key to provide insight and develop new therapeutic strategies for these diseases (7).

New breakthroughs in studying apoptosis regulation during B cell maturation have been made possible by the development of BH3 mimetics, a class of small molecular inhibitors that mimic proapoptotic proteins and have shown great promise as cancer therapeutics (8). In mice, naive and memory B cells are sensitive to the BH3 mimetic ABT-737, which inhibits BCL-2, BCL-X_L, and BCL-W, but pre-existing GC and plasma cells are resistant (9), suggesting that apoptosis is regulated differently at various stages of B cell maturation. Recently, human tonsillar GC B cells were found to be sensitive to MCL-1 inhibition, which supports previous findings that MCL-1 is essential for GC formation in mice (10, 11). Nonetheless, there remain challenges associated with studying apoptosis in primary human B cells, which have short life spans in culture, spontaneously undergo apoptosis, and are difficult to transfect. Additionally, how apoptotic regulation changes specifically during B cell activation is poorly understood. As a result, we used intracellular BH3 (iBH3) profiling to uncover the dominant antiapoptotic mechanism at the mitochondria of resting and activated primary human B cells (12, 13). The principles behind iBH3 profiling are based on the selective interactions between the pro- and antiapoptotic proteins of the Bcl2 family (14, 15). In short, the antiapoptotic proteins that are present at the mitochondria dictate which proapoptotic BH3-only peptides

Department of Molecular Genetics and Microbiology, Duke University School of Medicine, Durham, NC 27710; and Center for Virology, Duke University School of Medicine, Durham, NC 27710

Received for publication October 23, 2017. Accepted for publication December 18, 2017.

This work was supported by National Institutes of Health Grants R01-CA140337 and R01-DE025994 (to M.A.L.) and T32-CA009111 (to J.D.). Additional funding came from the Duke Center for AIDS Research, a National Institutes of Health-funded program (Grant 5P30-AI064518), and from American Cancer Society Grant RSG-13-228-01-MPC (both to M.A.L.).

J.D. and M.A.L. designed research; J.D. performed research; and J.D. and M.A.L. analyzed data and wrote the paper.

Address correspondence and reprint requests to Dr. Micah A. Luftig, Department of Molecular Genetics and Microbiology, Center for Virology, Duke University School of Medicine, 213 Research Drive, DUMC Box 3054, Durham, NC 27710. E-mail address: micah.luftig@duke.edu

The online version of this article contains supplemental material.

Abbreviations used in this article: CI, combination index; CTV, CellTrace Violet; GC, germinal center; iBH3, intracellular BH3; STS, staurosporine.

Copyright © 2018 by The American Association of Immunologists, Inc. 0022-1767/18/\$35.00

can induce mitochondrial depolarization and cytochrome *c* release. In this way, we can identify the antiapoptotic dependency, or Bcl2 dependency, of the sample. iBH3 profiling can also assay the Bcl2 dependency of multiple populations in heterogeneous samples, thereby eliminating the need for time-consuming and expensive sorting experiments to study rare populations (13).

With the advent of iBH3 profiling and BH3 mimetics, we are equipped with tools that allow us to study how apoptosis is regulated in human B cell subsets and activated B cells. Therefore, we have used iBH3 profiling to determine the BH3 profiles of normal, resting, and activated B cells, and validated the hypotheses generated by these profiles by treating normal and activated human B cell subsets with BH3 mimetics.

Materials and Methods

Cells and mitogens

Peripheral B cells were obtained from normal human donors through the Gulf Coast Regional Blood Center (Houston, TX). Buffy coats were layered over Ficoll–Histopaque-1077 gradient (H8889; Sigma-Aldrich) and washed three times with FACS buffer (5% FBS in PBS) and cultured in RPMI 1640 supplemented with 15% FBS (Corning), 2 mM L-glutamine, 100 U/ml penicillin, 100 µg/ml streptomycin (Invitrogen), and cyclosporin A. To track proliferation, PBMCs were stained with CellTrace Violet (CTV; C34557; Invitrogen) for 20 min in PBS at 37°C, washed in FACS buffer, and then cultured with the appropriate mitogens.

Tonsillar B cell subsets were obtained from discarded, anonymized tonsillectomies from the Duke Biospecimen Repository and Processing Core (Durham, NC). Tonsillectomies were manually disaggregated, filtered through a cell strainer, and isolated by Ficoll–Histopaque-1077 (H8889; Sigma-Aldrich). The harvested lymphocyte layer was washed three times with FACS buffer and cultured in RPMI 1640 supplemented with 15% FBS (Corning), 2 mM L-glutamine, 100 U/ml penicillin, 100 µg/ml streptomycin (Invitrogen), and cyclosporin A. For dose-response curves performed with S63845, tonsillar B cells were stained and sorted for CD19⁺ B cell subsets with a MoFlo Astrios cell sorter at the Duke Cancer Institute Flow Cytometry Shared Resource.

TLR9 ligand CpG oligonucleotide (ODN 2006) was purchased from Integrated DNA Technologies and used at 2.5 µg/ml (2). Human rIL-4 (AF200-04; ProProTech) was used at 20 ng/ml. Hemagglutinin-tagged CD40L (6420-CL; R&D Systems) was used at 5 ng/ml with an anti-hemagglutinin cross-linking peptide (MAB060; RRID: AB_10719128; R&D Systems) at a concentration of 0.2 µg/µl.

Intracellular BH3 profiling and validation

iBH3 profiling was performed with recombinant peptides synthesized by New England Peptides (sequences listed below). Stock peptides were resuspended at 10 mM in DMSO and aliquoted and stored at –80°C. To prepare peptides for iBH3 profiling, peptides were diluted to 200 µM in 0.004% digitonin in DTEB buffer (135 mM trehalose [T9449; Sigma-Aldrich], 20 µM EDTA [E6758; Sigma-Aldrich], 20 µM EGTA [E3889; Sigma-Aldrich], 5 mM succinic acid [S3674; Sigma-Aldrich], 0.1% IgG-free BSA [100182-742; VWR], 10 mM HEPES [H4034; Sigma-Aldrich], 50 mM potassium chloride [P9541; Sigma-Aldrich], adjusted to pH 7.5 with potassium hydroxide). Recombinant Bim peptide concentrations were used at 10, 1, and 0.1 µM. Alamethicin (BML-A150-0005; Enzo Life Sciences) was used at 25 µM.

PBMCs and tonsillar cells were iBH3 profiled immediately after processing, whereas mitogen-stimulated cells were profiled on day 6 post-stimulation. To prepare samples for iBH3 profiling, cells were stained with the Zombie Aqua viability dye (423101; BioLegend) in serum-free PBS for 15 min at room temperature and then stained with FACS Abs for surface markers for 30 min at 4°C. Because Zombie Aqua and CTV fluoresce in the same channel, mitogen-stimulated cells were centrifuged at low speed and washed to remove dead cells (i.e., trypan positive) before staining. After staining, cells were pelleted and resuspended at 4×10^6 cells/ml in DTEB buffer. Equal volumes (50 µl) of cells and peptides were incubated in polypropylene tubes for 1 h at room temperature in the dark. To stop the reaction, 30 µl of 4% paraformaldehyde in PBS was added and incubated at room temperature for 10 min. To neutralize the fixation, 30 µl of neutralization buffer (1.7 M Tris base, 1.25 M glycine [pH 9.1]) was added for 5 min. Intracellular levels of cytochrome *c* were probed by adding 20 µl of staining buffer (1% saponin, 10% BSA, 20% FBS, 0.02% sodium azide in PBS) with 1 µl of Ab for human cytochrome *c*. Samples were stained overnight and then transferred into polystyrene tubes for analysis the next day. The amino acid sequences of the recombinant peptides are (Ac, acetyl,

NH₂, amide): Bad, Ac-LWAAQRYGRELRRMSDEFEGSFKGL-NH₂; Bim, Ac-MRPEIWIQAQLRRIGDEFNA-NH₂; Bmf, Ac-HQAEVQIAR KLQLIADQFHRY-NH₂; Hrk, Ac-WSSAAQLTAARLKLALGDELHQ-NH₂; Noxa, Ac-AELPPEFAAQLRKIGDKVYC-NH₂; MS1, Ac-RPEIWMQ GLRRLGDEINAYAR-NH₂; Puma, Ac-EQWAREIGAQLRRMADDLNA-NH₂; Puma2A, Ac-EQWAREIGAQAARRMAADLNA-NH₂.

Flow cytometry

To track proliferation, cells were stained with CTV (C34557; Invitrogen). Cells were washed in FACS buffer (5% FBS in PBS), stained with fluorescently conjugated Abs for 30 min to 1 h at 4°C in the dark, and then washed again before being analyzed on a BD FACSCanto II. To normalize acquisition, Spherotech AccuCount (ACBP-50-10) beads were included in each tube. Abs used for flow cytometry are as follows: PE mouse anti-human IgD (555779, RRID:AB_396114; BD Pharmingen), allophycocyanin mouse anti-human CD38 (303510, RRID:AB_314362; BioLegend), PE-Cy7 mouse anti-human CD19 (25-0198-42, RRID: AB_10671548; eBioscience), FITC mouse anti-human cytochrome *c* (612304, RRID:AB_2090159; BioLegend), FITC mouse anti-human CD27 (555440, RRID:AB_395833; BD Pharmingen).

Dose-response curves and isobolograms

Small molecule inhibitors used in this study were ABT-737 (S1002; Selleckchem), ABT-199 (A12500; AdooQ Bioscience), WEHI-539 (A3935; ApexBio), A-1210477 (S7790; Selleckchem), S63845 (A8737; ApexBio), and staurosporine (STS; S5921-0.5MG; Sigma-Aldrich). Dose-response curves were generated by treating primary cells for 24 h at 37°C. Mitogen-activated cells were treated on day 3 poststimulation for 3 d and assayed on day 6. Counts of viable cells were determined by forward light scatter/side light scatter by flow cytometry and normalized to a DMSO, untreated (vehicle-only) control. Curves were drawn in GraphPad Prism 7 to calculate IC₅₀ values and 95% confidence intervals based on a Hill slope factor of 1.

Isobolograms were generated based on dose-response curves with individual drugs (drug 1, drug 2) and combinations of drugs (drug 1 plus drug 2) (29). Individual drug dose-response curves were used to identify drug concentrations at IC₃₀, IC₅₀, and IC₇₀. Similarly, at a constant concentration of drug 1, the concentrations of drug 2 were determined at the IC₃₀, IC₅₀, and IC₇₀ points of the combination dose-response curve. To calculate the combination index (CI), the following equation was used.

$$CI_{50} = \frac{[\text{Drug 1}] (IC_{50}, \text{ in combination})}{[\text{Drug 1}] (IC_{50}, \text{ alone})} + \frac{[\text{Drug 2}] (IC_{50}, \text{ in combination})}{[\text{Drug 2}] (IC_{50}, \text{ alone})}$$

The CI was also calculated for CI₃₀ (with IC₃₀ values) and for CI₇₀ (with IC₇₀ values). We classified the interaction between the combination of drugs based on the following CI values: CI > 1, antagonistic; CI = 1, additive; CI < 1, synergistic.

Protein expression

Mitogen-stimulated PBMCs were sorted on day 6 poststimulation on the MoFlo Astrios cell sorter at the Duke Cancer Institute Flow Cytometry Shared Resource. Cells were pelleted and washed in PBS and lysed in 0.1% Triton X-100-containing buffer with complete protease inhibitors (11697498001; Sigma-Aldrich). Protein lysates were run on NuPage 4–12% gradient gels (NP0322BOX; Thermo Fisher) in MES buffer and transferred to polyvinylidene difluoride membrane (GE Healthcare). Membranes were blocked in 5% milk in TBST and stained with primary Ab overnight at 4°C. Membranes were then washed in TBST and incubated with secondary Ab diluted in 5% milk in TBST for 1 h at room temperature. Protein levels were quantified by densitometry (Syngene) and normalized to β-actin levels. Abs used for protein expression are as follows: mouse anti-BCL-2 (BD551107; BD Biosciences), rabbit anti-MCL-1 (sc-819; Santa Cruz Biotechnology), rabbit anti-BCL-X_L (2762S; Cell Signaling Technology), rabbit anti-β-actin (600-401-886; Rockland Immunochemicals).

Gene expression analysis

Total RNA was isolated from cells by using a Qiagen RNeasy kit and reverse transcribed to generate cDNA with a high-capacity cDNA kit (4368814; Applied Biosystems). Quantitative PCR was performed by using SYBR Green (Quanta Biosciences) and run on an Applied Biosystems StepOnePlus instrument. Results were normalized to SetDB1. Oligonucleotides used for quantitative PCR

are as follows: BCL-2 (forward, 5'-GGTGGGGTCATGTGTGTGG-3', reverse, 5'-CGGTTTCAGGTACTCAGTCATCC-3'), BCL-X_L (forward, 5'-GAGCTGG TGGTTGACTTTCTC-3', reverse, 5'-TCCATCTCCGATTCAGTCCCT-3'), MCL-1 (forward, 5'-GTGCCTTTGTGGCTAAACACT-3', reverse, 5'-AGT CCCCCTTTGTCTTACGA-3'), BCL-W (forward, 5'-GCGGAGTTCA-CAGCTCTATAC-3', reverse, 5'-AAAAGGCCCTACAGTTACCA-3'), BFL-1 (forward, 5'-TTACAGGCTGGCTCAGGACT-3', reverse, 5'-AGCACTCTG-GACGTTTTGCT-3'), SetDB1 (forward, 5'-TCCATGGCATGCTGGAGCGG-3', reverse, 5'-GAGAGGGTCTTGGCCCGGT-3').

Statistical analysis

A Student two-way ANOVA and two-tailed *t* test were calculated using GraphPad Prism 5.0 software. A *p* value < 0.05 was considered significant. IC₅₀ values were calculated by nonlinear regression using GraphPad, and 95% confidence intervals were reported.

Results

Preswitched and switched human B cells circulating in the periphery depend on BCL-2 for survival

We sought to determine the mechanism of apoptosis regulation in human peripheral blood B cells from within the bulk PBMC population (12). After staining for cell-specific surface markers, cells were incubated with recombinant BH3-only peptides and digitonin, which selectively permeabilizes the outer cellular membrane and exposes intact mitochondria to the peptide treatment (Fig. 1A). Following peptide treatment, the cells were fixed, incubated with saponin to permeabilize mitochondria, and stained with a fluorescently labeled Ab to quantify the remaining levels of intracellular cytochrome *c*. The extent of cytochrome *c* release was measured as the dynamic range between total levels of cytochrome *c*, determined by treating with an inert recombinant PUMA BH3-only peptide (PUMA2A) and alamethicin, which can induce 100% cytochrome *c* release.

Initially, we identified the antiapoptotic dependencies of pre-switched and switched B cells in PBMCs. Preswitched (CD19⁺IgD⁺) and switched (CD19⁺IgD⁻) B cells were distinguished by IgD expression (Fig. 1B). iBH3 profiling revealed that the mitochondria in preswitched and switched B cells in the peripheral blood were highly sensitive to BIM, BAD, PUMA, and BMF, moderately sensitive to HRK, and relatively resistant to NOXA (Fig. 1C). This pattern of sensitivity, along with previously published reports in mice (9), suggested that both preswitched and switched B cells were dependent on BCL-2 for survival, but the moderate sensitivity to HRK also suggested a dependency on BCL-X_L for survival (Fig. 1D).

To validate these hypotheses and distinguish between BCL-2 and BCL-X_L dependency, we treated PBMCs with the following BH3 mimetics: ABT-737 (BCL-2, BCL-X_L, BCL-W inhibitor), ABT-199 (BCL-2 inhibitor), or WEHI-539 (BCL-X_L inhibitor) (Fig. 1E). Preswitched and switched B cells were both sensitive to ABT-737 and ABT-199 (IC₅₀ < 1 μM), although switched (CD19⁺IgD⁻) B cells were less sensitive than preswitched B cells to BCL-2 inhibition. This could be explained by their iBH3 profile, in which switched B cells were slightly more responsive to the HRK peptide and therefore possibly more dependent on BCL-X_L. However, both subsets were resistant to WEHI-539 (IC₅₀ > 1 μM), therefore confirming that preswitched and switched B cells are exclusively dependent on BCL-2 for survival. This also corroborates previously published results of BCL-2 dependency in murine naive and memory B cells from the periphery and highlighting the importance of using BH3 mimetics in validating hypotheses posed by iBH3 profiling (Fig. 1F) (9). The observed sensitivities of preswitched and switched B cells to ABT-199 also precluded the possibility of either subset being dependent on BCL-W, which has identical binding partners as BCL-2 (Fig. 1D).

Finally, we found that both B cell subsets were equally capable of undergoing BAX/BAK-dependent apoptosis based on their sensitivity to the pan-kinase inhibitor STS (16).

Because preswitched B cells included both naive and non-switched memory B cells, we also assessed the sensitivities to BH3 mimetics in B cell subsets costained for IgD and CD27. Interestingly, we found that nonswitched memory B cells (CD19⁺IgD⁺CD27⁺) were equally sensitive to BCL-2 inhibition as naive B cells (CD19⁺IgD⁺CD27⁻) (Supplemental Fig. 1). Both of these IgD⁺ populations were more sensitive than the switched memory population (CD19⁺IgD⁻CD27⁺), and all three populations were resistant to WEHI-539 (Supplemental Fig. 1).

B cell maturation is associated with changes in Bcl-2 family dependency

To determine the changes in apoptotic regulation that take place during human B cell maturation, we queried the apoptotic regulation of CD19⁺ naive (IgD⁺CD38⁻), memory (IgD⁻CD38⁻), GC (IgD⁻CD38^{mid}) B cells, and plasma cells (IgD⁻CD38^{hi}) from tonsillar tissue (Fig. 2A). Similar to naive and memory B cells in peripheral blood, tonsillar naive and memory B cells were highly sensitive to BIM, BAD, PUMA, and BMF and were predicted to be BCL-2-dependent (Fig. 2B, 2C). GC B cells, however, had a modestly lower response to BAD and a significantly heightened response to NOXA, suggesting that GC B cells were dependent on MCL-1 for survival. Plasma cells were much less responsive to BH3 peptide treatments compared with the other B cell subsets. However, we hypothesized that within the reduced dynamic range of plasma cell responses, lower NOXA sensitivity as compared with BAD and HRK suggested dependence on BCL-X_L for survival.

To validate the hypotheses generated from iBH3 profiling, we treated primary tonsillar B cells with ABT-199, ABT-737, WEHI-539, and STS (Fig. 2D, 2E). All cells were sensitive to STS, indicating that all subsets were capable of intrinsic apoptosis. As predicted, naive and memory B cells were sensitive to BCL-2 inhibition by ABT-199 and ABT-737. Plasma cells were uniquely sensitive to BCL-X_L inhibition by WEHI-539, confirming their dependence on BCL-X_L. The difference in the sensitivity of plasma cells to ABT-737 and WEHI-539 may be due to a difference in their binding affinities for BCL-X_L (ABT-737 IC₅₀ = 35 nM versus WEHI-539 IC₅₀ = 1.1 nM) (8, 17). GC B cells were resistant to ABT-737, ABT-199, and WEHI-539 because none of these drugs inhibited MCL-1. However, GC B cells were also resistant to the MCL-1-specific BH3 mimetic A-1210477, but display selective sensitivity to low doses of S63845, which binds to MCL-1 with greater affinity than does A-1210477 (Supplemental Fig. 2A, 2B) (18, 19). Furthermore, when tonsillar B cells were iBH3 profiled with low doses of S63845 and MS1, an engineered recombinant peptide with higher affinity and specificity for MCL-1 than NOXA (20), the mitochondria of GC B cells were significantly more responsive to MCL-1 antagonism than were the other subsets (Supplemental Fig. 2C). In sum, MCL-1 regulates the survival of GC B cells. These findings support an existing model that B cells adjust their Bcl-2 family dependency throughout T-dependent B cell maturation. Moreover, iBH3 profiling proved to be reliable in querying Bcl-2 family dependencies in heterogeneous cell populations.

CD40L/IL-4-stimulated B cells are sensitive to NOXA and HRK peptides, yet remain sensitive to BCL-2 inhibition

We next sought to model B cell maturation with mitogen stimulation of peripheral blood B cells. To track proliferation, PBMCs were stained with CTV, which becomes diluted upon cell division (Fig. 3A).

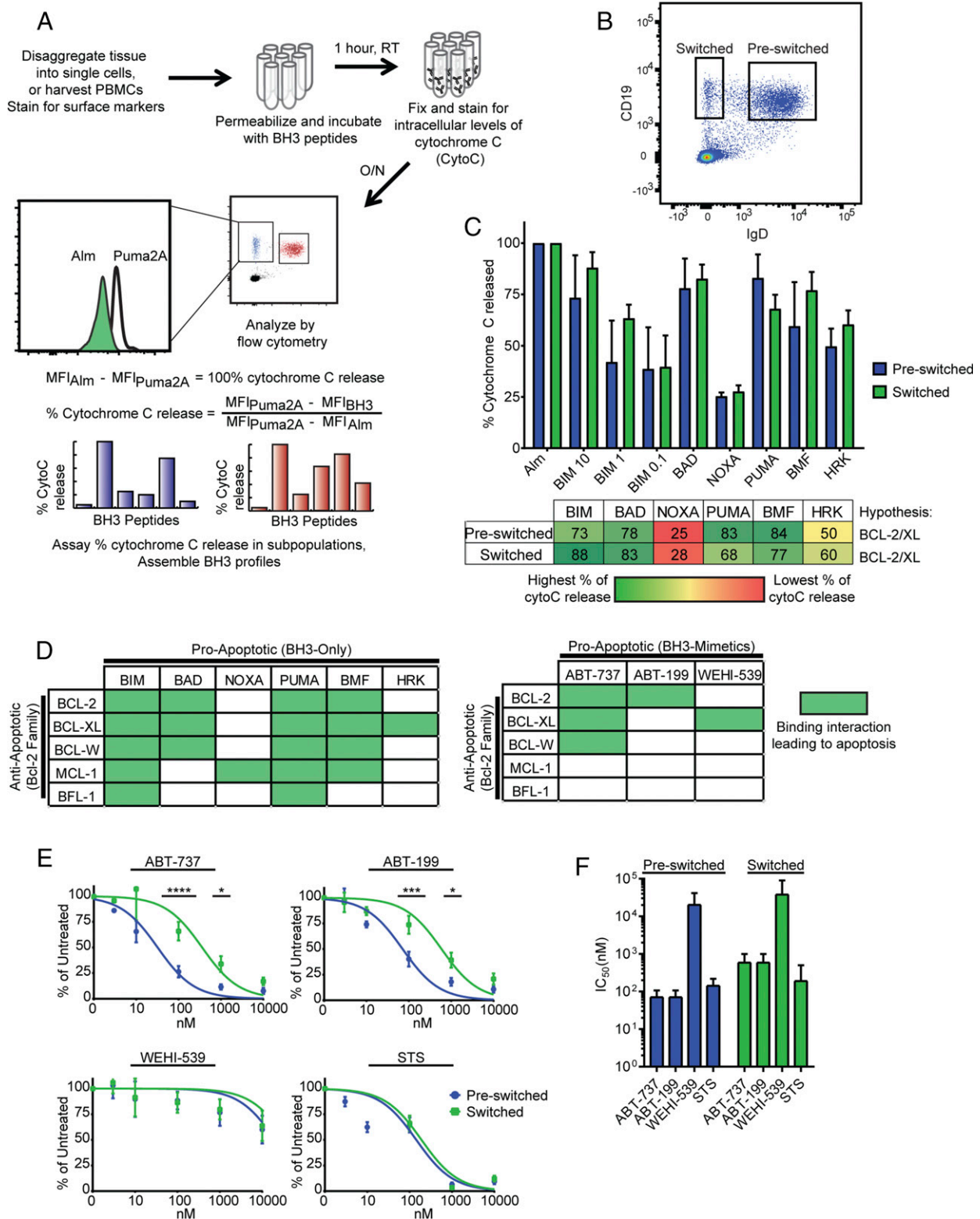


FIGURE 1. The iBH3 profiles of normal, resting human B cells from the peripheral blood. **(A)** Schematic of the iBH3 process, including how the percentage of cytochrome *c* release is quantified. **(B)** Representative flow cytometry plot of CD19⁺ naive (IgD⁺) and memory B cells (IgD⁻) from human PBMCs. **(C)** iBH3 profiles of naive and memory B cells from three human donors. Mean and SEM are plotted; mean values are summarized in table below. Percentage of cytochrome *c* release is normalized to alamethicin (Alm) as positive control and Puma2A as negative control. BIM 10, 10 μM BIM; BIM 1, 1 μM BIM; BIM 0.1, 0.1 μM BIM. **(D)** Left, schematic of selective interactions between pro- and antiapoptotic members of the Bcl-2 protein family and, right, BH3 mimetics and the antiapoptotic proteins that they inhibit. Green boxes indicate a binding interaction between the two proteins that leads to cytochrome *c* release. **(E)** Dose-response curves generated from treating PBMCs for 24 h with ABT-737 (BCL-2, BCL-X_L, BCL-W inhibitor; eight human donors), ABT-199 (BCL-2 inhibitor; eight human donors), WEHI-539 (BCL-X_L inhibitor; three human donors), and STS (naive, nine human donors; memory, eight human donors), a broad kinase inhibitor that can induce apoptosis. Percentage survival is measured as a percentage of DMSO-treated controls. Mean and SEM are plotted, and statistical analyses were performed by two-way ANOVA. At 100 nM ABT-737, *****p* < 0.0001; at 1000 nM, **p* = 0.0337. At 100 nM ABT-199, ****p* = 0.0002; at 1000 nM, **p* = 0.0383. **(F)** Average IC₅₀ values with 95% confidence intervals for naive and memory B cells are plotted from (E).

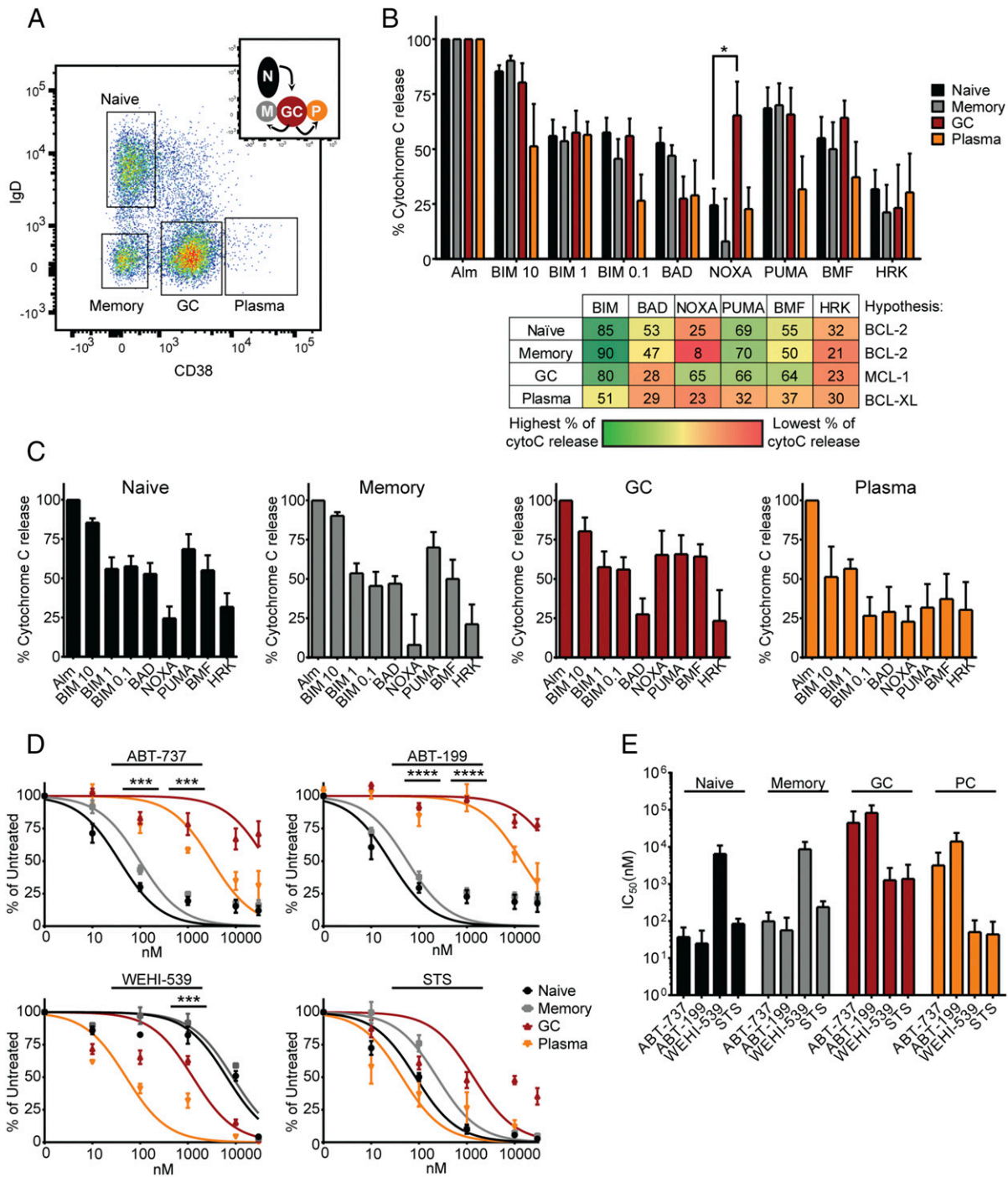


FIGURE 2. The iB3 profiles of normal, resting human B cells from tonsillar lymphoid tissue. **(A)** Representative flow cytometry plot of CD19⁺ B cell subsets found in human tonsillar tissue: naive (IgD⁺ CD38⁻), memory (IgD⁻ CD38⁺), GC (IgD⁻ CD38^{mid}), and plasma cells (IgD⁻ CD38^{hi}). Inset, a color-coded schematic of the GC reaction. **(B)** iB3 profiles of tonsillar B cell subsets from four to five human donors. Mean and SEM are plotted; mean values are summarized in the table below. Percentage of cytochrome *c* release is normalized to alamethicin (Alm) as positive control and Puma2A as negative control. In samples treated with Noxa-derived recombinant peptides, **p* = 0.0467, by an unpaired two-tailed Student *t* test. **(C)** Same as in (B), but showing each subset's profile individually. **(D)** Dose-response curves generated from treating disaggregated tonsils for 24 h with ABT-737 (BCL-2, BCL-X_L, BCL-W inhibitor; three human donors), ABT-199 (BCL-2 inhibitor; three human donors), WEHI-539 (BCL-X_L inhibitor; three human donors), and STS (four to six human donors), a broad kinase inhibitor that can induce apoptosis. Percentage survival is measured as a percentage of DMSO-treated controls. Mean and SEM are plotted, and statistics were performed by a two-way ANOVA with multiple comparisons. At 100 and 1000 nM ABT-737: naive versus GC, naive versus plasma, and memory versus GC, *****p* < 0.0001. Memory versus plasma, ****p* = 0.0003. Naive versus memory and GC versus plasma were not significant. At 100 and 1000 nM ABT-199, naive versus GC, naive versus plasma, memory versus GC, and memory versus plasma, *****p* < 0.0001. Naive versus memory and GC versus plasma were not significant. At 1000 nM WEHI-539, naive versus GC, ****p* = 0.0009. Naive versus plasma, memory versus GC, memory versus plasma, GC versus plasma, *****p* < 0.0001. Naive versus GC, ****p* = 0.0009. Naive versus memory was not significant. **(E)** Average IC₅₀ values with 95% confidence intervals for each subset are plotted from (D). PC, plasma cell.

CTV was retained during permeabilization with digitonin, thereby making it suitable in iB3 profiling. We induced proliferation in peripheral blood B cells ex vivo by treating with CD40L and IL-4 to

mimic T cell-derived signals important in B cell survival in the GC. CD19⁺ B cells began proliferating 3 d after treatment with CD40L/IL-4, as shown previously (21, 22).

CD40L/IL-4-stimulated B cells were iBH3 profiled 6 d post-stimulation (Fig. 3B). Proliferating B cells displayed modestly increased sensitivity to NOXA and HRK peptide treatment relative to nonproliferating B cells, suggesting an increasing dependence on MCL-1 and BCL-X_L for survival. This hypothesis is also bolstered by increased expression of MCL-1 protein and BCL-X_L mRNA in proliferating naive and memory B cells compared with nonproliferating B cells (Fig. 3C, 3D). MCL-1 expression is tightly regulated, and observed increases in MCL-1 protein levels in proliferating B cells may be due to posttranslational modifications that can rapidly upregulate MCL-1 protein stability and total protein levels without increasing mRNA levels (11, 23, 24). Interestingly, BCL-2 mRNA and protein levels remain relatively consistent among proliferating and nonproliferating subsets.

The robust increase in HRK sensitivity in the iBH3 profiling assay correlated with increased susceptibility of proliferating B cells to the BCL-X_L inhibitor WEHI-539 (Fig. 3E, 3F). However, these cells remained moderately sensitive to ABT-199 and ABT-737 ($0.1 \mu\text{M} < \text{IC}_{50} < 1 \mu\text{M}$), suggesting that BCL-2 still plays an important role in CD40L/IL-4-stimulated B cell survival (Fig. 3E, 3F). Furthermore, in proliferating subsets, there is an increase in sensitivity to low doses of BIM, suggesting an increase in “priming” or overall sensitivity to apoptosis (15). This increase in priming could offset the increase in NOXA sensitivity observed in proliferating B cells that would otherwise confer MCL-1 dependence and subsequent resistance to BCL-2 inhibitors. As a result, nonproliferating and proliferating subsets are equally sensitive to BCL-2 inhibition. Finally, proliferating subsets are more sensitive to STS compared with nonproliferating B cells (Fig. 3E, 3F), most likely due to inhibition of kinase activity induced by CD40 ligation (25, 26).

A CD38^{hi}, plasmablast-like subpopulation in CpG-stimulated B cells becomes sensitive to NOXA and HRK in iBH3 profiling and becomes resistant to BCL-2 inhibition

In B cells activated to proliferate *ex vivo* by CpG DNA, a pathogen-associated molecular pattern that stimulates the TLR9 pathway, we observed similar changes in apoptotic regulation in proliferating B cells. However, in CpG-stimulated cells, a subset of B cells that have undergone the most cellular divisions upregulate high levels of CD38 surface expression, suggesting that they have differentiated into plasmablast-like B cells (CTV^{lo}CD38^{hi}; Fig. 4A) (3, 27). This population consisted predominantly of IgD⁻ memory B cells (~80–95%) and is noticeably absent in CD40L/IL-4-stimulated B cells because IL-4 promotes differentiation of memory B cells (CD38^{lo}) over plasma cells (CD38^{hi}) (28). Nonetheless, not all proliferating B cells upregulated CD38 expression, and the CTV^{lo}CD38^{lo} population included both IgD⁺ (naive) and IgD⁻ (memory) B cells. In iBH3 profiling of CpG-stimulated B cells, nonproliferating B cells were predicted to be BCL-2-dependent (Fig. 4B). As they proliferate they become more responsive to NOXA and HRK peptides, with CD38^{hi} B cells as the most responsive to NOXA and HRK (Fig. 4B). The increased sensitivity to NOXA and HRK can further be explained by increased expression at the protein and mRNA levels of MCL-1 and BCL-X_L, which NOXA and HRK antagonize, respectively (Fig. 4C, 4D). Additionally, BCL-2 protein levels were reduced in proliferating subsets compared with nonproliferating B cells, suggesting that the antiapoptotic dependency in proliferating B cells switches from BCL-2 to a combination of MCL-1 and BCL-X_L (Fig. 4C, 4D).

To test this hypothesis, we treated CpG-stimulated B cells with BH3 mimetics. Nonproliferating and CD38^{lo} proliferating B cells were within the same range of sensitivity to ABT-199 and ABT-

737 and were refractory to WEHI-539, indicating that as B cells proliferated in response to CpG, BCL-2 remained important in regulating survival (Fig. 4E, 4F). CD38^{hi} B cells, in contrast, were less sensitive to ABT-199 and ABT-737 and were slightly more sensitive to WEHI-539.

The overall increase in apoptosis resistance in the CD38^{hi} subset is not because of impaired BAX and BAK activation, because CD38^{hi} cells were sensitive to STS, but rather it may be due to an increasing dependence on MCL-1 as indicated by increasing sensitivity to NOXA in their iBH3 profile. In fact, of the proliferating subsets, the response of the CD38^{hi} subset to NOXA was significantly different from that of nonproliferating B cells ($p = 0.0292$). Thus, to inhibit both BCL-X_L and MCL-1, we tested the efficacy of combining WEHI-539 with A-1210477 in CpG-stimulated PBMCs (29). CpG-stimulated B cells were refractory to high concentrations of A-1210477 (Supplemental Fig. 3A, 3B). However, a combination of A-1210477 and sub-IC₅₀ levels of WEHI-539 resulted in synergism ($\text{CI} < 1$) in the CD38^{hi} subpopulation (Supplemental Fig. 3C). This effect was specific to MCL-1, as ABT-199 did not synergize with WEHI-539 ($\text{CI} \approx 1$) (Supplemental Fig. 3D).

Discussion

Proper regulation of apoptosis is critical for B lymphocyte development and maturation. Much of our mechanistic understanding of B cell apoptosis is derived from murine studies due to technical limitations in studying B cell subsets in humans (9, 10, 30). Two recent studies have characterized Bcl-2 family dependency in human primary and secondary lymphoid tissue (11, 31). Sarosiek et al. (31) characterized how apoptosis is regulated in healthy tissues, from young and aged mouse models, and found that younger tissues, which often have higher levels of c-Myc activity, are more sensitive to apoptosis and subsequent mitochondrial outer membrane permeabilization. Similar to their study, ours identified dynamic apoptotic regulation that occurs during development; however, Sarosiek et al. used a plate-based BH3 profiling method on homogenized tissues whereas we used a FACS-based intracellular version of BH3 profiling that allows us to characterize the apoptotic regulation of heterogeneous tissues.

Peperzak et al. (30) used “BH3 mimetic profiling,” in which they used BH3 mimetics to query the antiapoptotic mechanisms in B cell subsets and in cell lines derived from chronic lymphocytic leukemia. In short, this is the method that we used to verify the hypotheses generated by iBH3 profiling. Our work both corroborated and strengthened Peperzak et al.’s results showing that GC B cells upregulate MCL-1 expression and are sensitive to MCL-1 inhibition by A-1210477. With iBH3 profiling, we showed that the mitochondria of GC B cells are extremely sensitive to apoptosis induced by the BH3-only peptide NOXA, which selectively binds MCL-1, as well as the NOXA-derived peptide MS1 and a new MCL-1 inhibitor S63845. This suggests that, functionally, MCL-1 is a critical regulator of survival at the mitochondrial surface of GC B cells.

Furthermore, another distinction between our work and others is that we characterize the changes in apoptotic regulation that accompany proliferation and differentiation in B cells stimulated by cytokines *in vitro*. By using a proliferation tracking dye, we have expanded upon the utility of iBH3 profiling. Ultimately, changes in apoptotic regulation occur in response to intracellular stress that accrues due to proliferation and differentiation.

In this study, we used the newly developed iBH3 profiling technique to query the mechanisms underlying apoptotic regulation both in heterogeneous lymphoid tissue as well as upon activation of normal B cell subsets *ex vivo* (13, 32). Our experimental approach

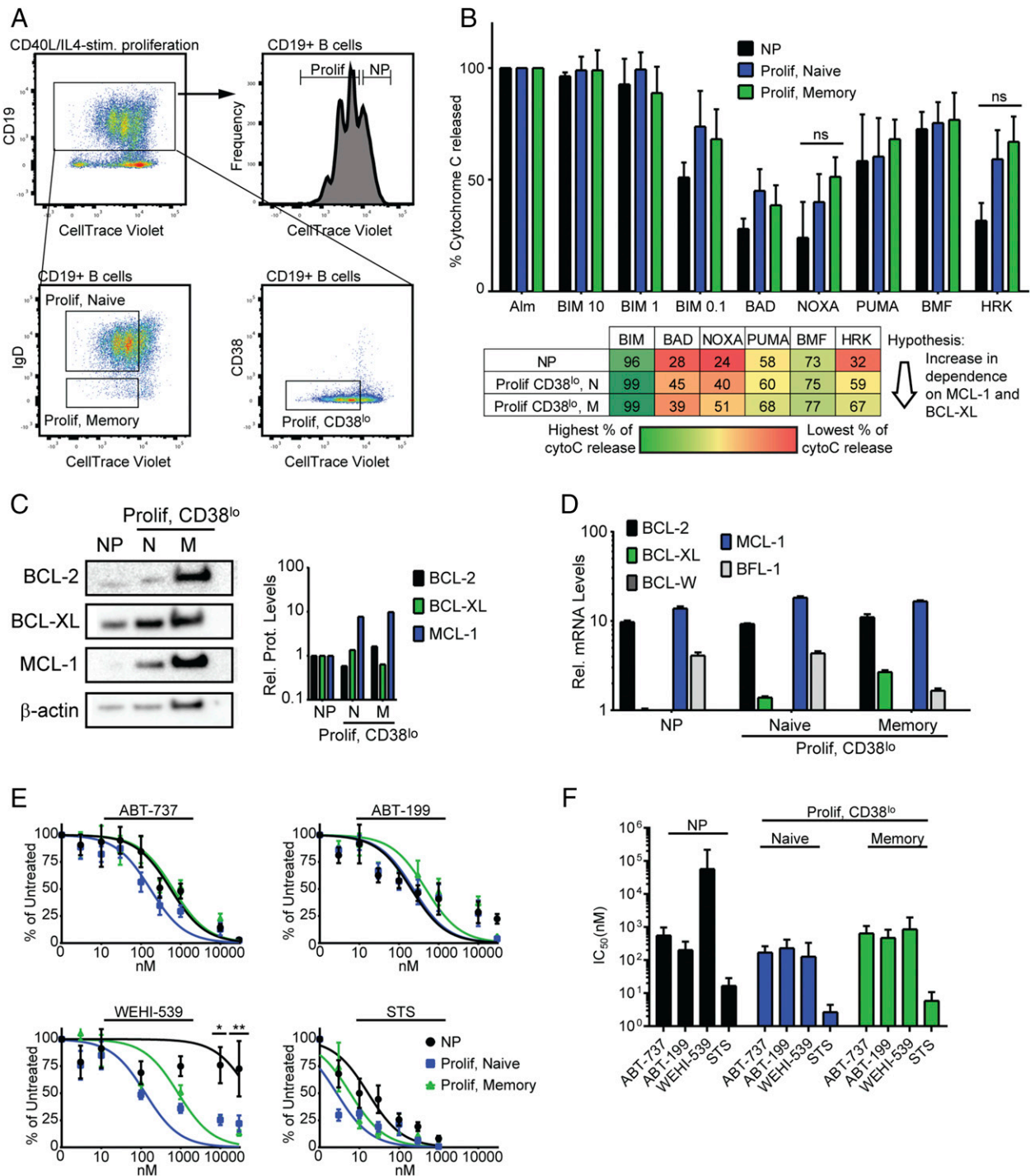


FIGURE 3. Changes in apoptotic regulation in activated, proliferating B cells stimulated by CD40L/IL-4. **(A)** Representative flow cytometry plot of CD19⁺ B cells that have been stimulated to proliferate by CD40L/IL-4, day 7 after stimulation. Dilution of CTV with each division distinguishes proliferating (Prolif; CTV^{lo}) cells from nonproliferating (NP; CTV^{hi}) cells. Cells that have proliferated the furthest also upregulate CD38 surface expression to some extent, but the size of this population has been inconsistent across donors. Both naive and memory B cells proliferate in response to CD40L/IL-4 stimulation. **(B)** iBH3 profiles of different subsets of CD40L/IL-4-stimulated B cells from three to five human donors. Mean and SEM are plotted; mean values are summarized in the table below. Percentage of cytochrome *c* release is normalized to alamethicin as positive control and Puma2A as negative control. ns, not significant by unpaired two-tailed Student *t* test. **(C)** Representative Western blot of nonproliferating (NP), proliferating naive (N), and proliferating memory (M) B cells sorted from CD40L/IL-4-stimulated B cells day 6 posttreatment. Quantified protein levels are normalized to the nonproliferating subset and β -actin. **(D)** Quantitative PCR of antiapoptotic genes from subsets sorted from CD40L/IL-4-stimulated B cells. mRNA was isolated from three biological donors and values were normalized to SetDB1. **(E)** Dose-response curves generated from treating three human donors for 3 d with ABT-737 (six human donors), ABT-199 (four to nine human donors), WEHI-539 (three human donors), and STS (six human donors). Mean and SEM are plotted, and statistics were performed by two-way ANOVA with multiple comparisons. At 10,000 nM WEHI-539, NP versus Prolif. CD38^{lo} naive, $**p = 0.0060$; NP versus Prolif. CD38^{lo} memory, $*p = 0.0101$. At 30,000 nM WEHI-539, NP versus Prolif. CD38^{lo} naive, $**p = 0.0060$; NP versus Prolif. CD38^{lo} memory, $**p = 0.0012$. **(F)** Average IC₅₀ values with 95% confidence intervals for each subset are plotted from (E).

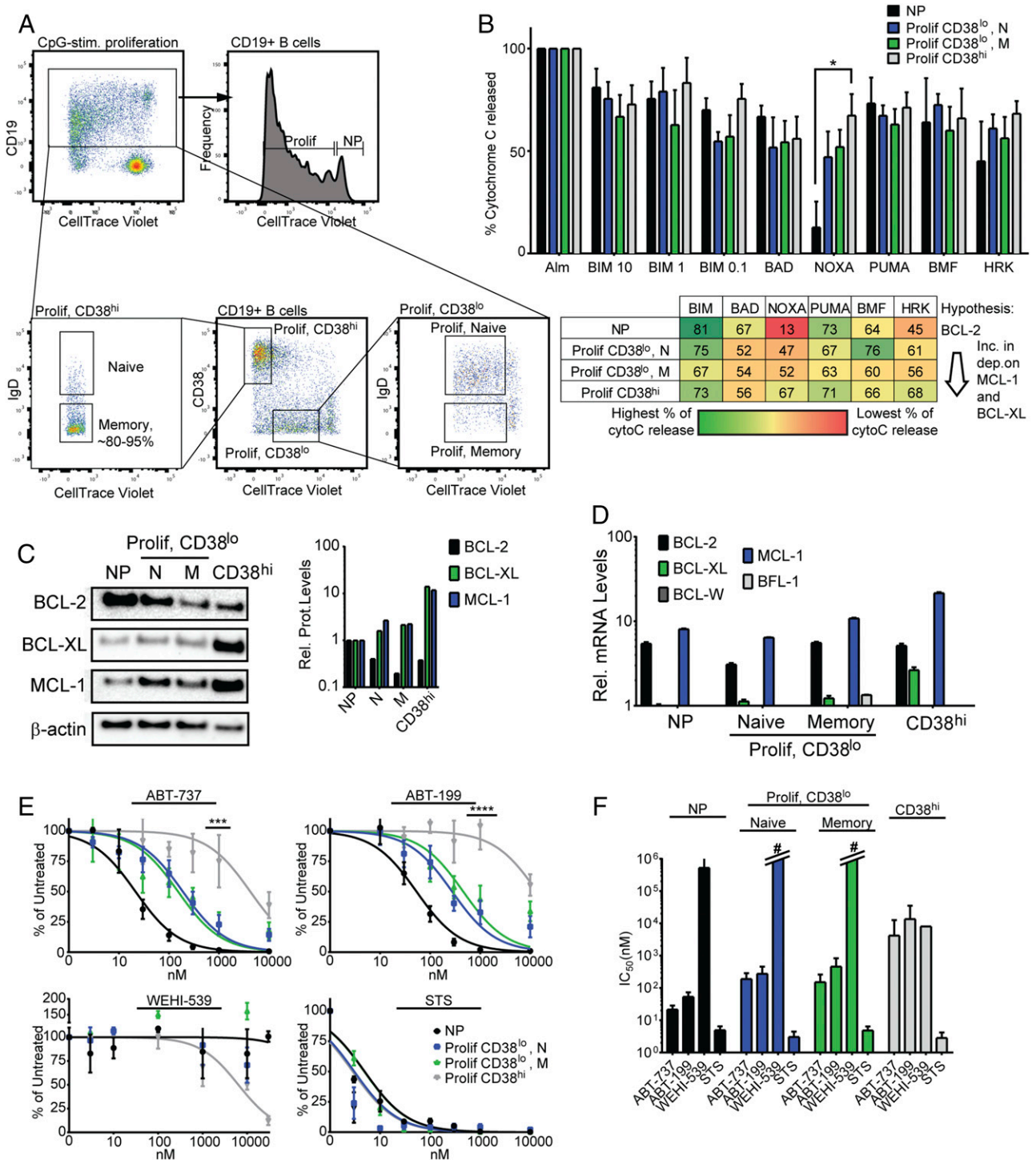


FIGURE 4. Changes in apoptotic regulation in activated, proliferating B cells stimulated by CpG. **(A)** Representative flow cytometry plot of CD19⁺ B cells that have been stimulated to proliferate by CpG, day 6 after stimulation. Dilution of CTV with each division distinguishes proliferating (Prolif) cells from nonproliferating (NP) cells. Cells that have proliferated the most also upregulate high CD38 surface expression (CD38^{hi}). Both naive and memory B cells proliferate in response to CpG stimulation. **(B)** iBH3 profiles of different subsets of CpG-stimulated B cells from four human donors. Mean and SEM are plotted; mean values are summarized in the table below. Percentage of cytochrome *c* release is normalized to alamethicin (Alm) as positive control and Puma2A as negative control. In samples treated with Noxa-derived peptide, **p* = 0.0292, by unpaired two-tailed Student *t* test. **(C)** Representative Western blot of nonproliferating (NP), proliferating CD38^{lo} naive (N) and memory (M) B cells, and CD38^{hi} B cells sorted from CpG-stimulated B cells at day 6 posttreatment. Quantified protein levels are normalized to the nonproliferating subset and β-actin. **(D)** Quantitative PCR of antiapoptotic genes from subsets sorted from CpG-stimulated B cells. mRNA was isolated from three biological donors and values were normalized to SetDB1. **(E)** Dose-response curves generated from CpG-stimulated PBMCs for 3 d with ABT-737 (five to seven human donors), ABT-199 (five to seven human donors), WEHI-539 (three human donors), and STS (six to seven human donors). Mean and SEM are plotted, and statistics are performed by two-way ANOVA, multiple comparisons. At 1000 nM ABT-737, NP versus CD38^{hi}, *****p* < 0.0001; CD38^{hi} versus Prolif CD38^{lo} naive, ****p* < 0.001; CD38^{hi} versus Prolif CD38^{lo} memory, ****p* < 0.001. At 1000 nM ABT-199, CD38^{hi} versus the three other subsets, *****p* < 0.0001. **(F)** Average IC₅₀ values with 95% confidence intervals for each subset are plotted from **(E)**. #For these subsets, there is no detectable sensitivity and therefore no calculable IC₅₀ value.

coupled proliferation tracking with cell surface markers to measurement of intracellular cytochrome *c* release in response to BH3 peptides to define Bcl2 family member dependency at the single cell level in heterogeneous B cell populations. The addition of a proliferation tracking dye expanded upon the utility of iBH3 profiling and allowed us to characterize changes in apoptotic regulation due to proliferation in *in vitro* experiments.

Validation of iBH3 profiling with BH3 mimetics defined transitions during B cell maturation from BCL-2 dependency in naive and memory B cells to MCL-1 in GC B cells, and to BCL-X_L in plasma cells from secondary lymphoid tissue. Then, upon stimulation by CpG or CD40L/IL-4, the Bcl2 dependency of proliferating B cells shifts from BCL-2 to a combination of BCL-X_L and MCL-1. This shift is apparent by the increased resistance to BCL2-specific BH3 mimetics and is most pronounced in the most differentiated subset of CpG-stimulated B cells.

Our findings corroborate several *in vivo* studies in mice that suggest that stage-specific Bcl2 dependency occurs throughout B cell maturation. Our work indicates that human naive and memory B cells, similar to those in mice, are sensitive to BCL-2 inhibition, whereas GC and plasma cells are refractory (9). In mouse GC B cells or those induced to differentiate into plasma cells *ex vivo*, MCL-1 is important in promoting survival (10, 30). Furthermore, murine plasma cells depend on BCL-X_L protection from apoptosis due to the unfolded protein response (33). These parallels in mouse studies with our findings in human B cells suggest that intrinsic apoptotic regulation in B cell maturation is highly conserved and functionally critical to humoral immunity.

Proliferating B cells in the GC as well as *ex vivo* mitogen-stimulated B blasts display evidence of oxidative and metabolic stress as well as DNA damage, which if left unresolved can lead to apoptosis (21, 34–36). Our findings indicate that GC cells display a heightened response to NOXA in iBH3 profiling, suggesting an increased dependence on MCL-1. Additionally, our laboratory has found that following EBV infection of primary human B cells, which is characterized by hyperproliferation and activation of the DNA damage response (37), there is a shift in Bcl2 dependency from BCL-2 to MCL-1 (38). This suggests that upon proliferation, MCL-1 expression is rapidly induced to respond to apoptosis-inducing intracellular stress resulting from rapid expansion and differentiation.

Constitutive activation of gene expression and survival programs found in normal B cell maturation can promote the development of lymphomas. For example, in follicular lymphoma, a t(14;18) chromosomal translocation induces BCL-2 overexpression in naive B cells, thereby promoting survival in the B cell follicle of a GC (39, 40). Consistent with our findings and those of others linking GC survival to MCL-1 upregulation (10, 11), a subset of diffuse large B cell lymphomas that arise from the GC often display MCL-1 copy number gains (41). Indeed, c-Myc-driven Burkitt lymphomas are thought to have arisen from GC B cells, express high levels of MCL-1, and are sensitive to MCL-1 inhibition (19, 42–44). MCL-1 is also often overexpressed in plasma cell-derived multiple myelomas, mimicking the requisite upregulation of MCL-1 induced by stromal interactions in the bone marrow (45, 46). Interestingly, a subset of plasma cell-derived tumors also displays codependence of MCL-1 and BCL-X_L (47), similar to our findings in CpG-induced CD38^{hi} plasmablasts. Overall, these data strongly support the importance of defining B cell survival mechanisms in normal and mitogen-stimulated human B cells toward understanding the underlying basis of B lymphoma cell survival.

Acknowledgments

We thank Lynn Martinek, Nancy Martin, and Mike Cook for extensive help in flow-based cytometry experiments and Karyn McFadden, Alex Price, and Nick Homa for critical reading of the manuscript. Special thanks to Jeremy Ryan from the Letai laboratory for technical help.

Disclosures

The authors have no financial conflicts of interest.

References

- Bortnick, A., and D. Allman. 2013. What is and what should always have been: long-lived plasma cells induced by T cell-independent antigens. *J. Immunol.* 190: 5913–5918.
- Krieg, A. M., A. K. Yi, S. Matson, T. J. Waldschmidt, G. A. Bishop, R. Teasdale, G. A. Koretzky, and D. M. Klinman. 1995. CpG motifs in bacterial DNA trigger direct B-cell activation. *Nature* 374: 546–549.
- Bernasconi, N. L., E. Traggiai, and A. Lanzavecchia. 2002. Maintenance of serological memory by polyclonal activation of human memory B cells. *Science* 298: 2199–2202.
- Victoria, G. D., and M. C. Nussenzweig. 2012. Germinal centers. *Annu. Rev. Immunol.* 30: 429–457.
- Peperzak, V., I. B. Vikstrom, and D. M. Tarlinton. 2012. Through a glass less darkly: apoptosis and the germinal center response to antigen. *Immunol. Rev.* 247: 93–106.
- Fischer, U., R. U. Jänicke, and K. Schulze-Osthoff. 2003. Many cuts to ruin: a comprehensive update of caspase substrates. *Cell Death Differ.* 10: 76–100.
- Vo, T. T., J. Ryan, R. Carrasco, D. Neuberger, D. J. Rossi, R. M. Stone, D. J. Deangelo, M. G. Frattini, and A. Letai. 2012. Relative mitochondrial priming of myeloblasts and normal HSCs determines chemotherapeutic success in AML. *Cell* 151: 344–355.
- Oltsersdorf, T., S. W. Elmore, A. R. Shoemaker, R. C. Armstrong, D. J. Augeri, B. A. Belli, M. Bruncko, T. L. Deckwerth, J. Dinges, P. J. Hajduk, et al. 2005. An inhibitor of Bcl-2 family proteins induces regression of solid tumours. *Nature* 435: 677–681.
- Carrington, E. M., I. B. Vikstrom, A. Light, R. M. Sutherland, S. L. Londrigan, K. D. Mason, D. C. Huang, A. M. Lew, and D. M. Tarlinton. 2010. BH3 mimetics antagonizing restricted pro-survival Bcl-2 proteins represent another class of selective immune modulatory drugs. *Proc. Natl. Acad. Sci. USA* 107: 10967–10971.
- Vikstrom, I., S. Carotta, K. Lüthje, V. Peperzak, P. J. Jost, S. Glaser, M. Busslinger, P. Bouillet, A. Strasser, S. L. Nutt, and D. M. Tarlinton. 2010. Mcl-1 is essential for germinal center formation and B cell memory. *Science* 330: 1095–1099.
- Peperzak, V., E. Slinger, J. Ter Burg, and E. Eldering. 2017. Functional disparities among BCL-2 members in tonsillar and leukemic B-cell subsets assessed by BH3-mimetic profiling. *Cell Death Differ.* 24: 111–119.
- Ryan, J. A., J. K. Brunelle, and A. Letai. 2010. Heightened mitochondrial priming is the basis for apoptotic hypersensitivity of CD4⁺ CD8⁺ thymocytes. *Proc. Natl. Acad. Sci. USA* 107: 12895–12900.
- Ryan, J., J. Montero, J. Rocco, and A. Letai. 2016. iBH3: simple, fixable BH3 profiling to determine apoptotic priming in primary tissue by flow cytometry. *Biol. Chem.* 397: 671–678.
- Youle, R. J., and A. Strasser. 2008. The BCL-2 protein family: opposing activities that mediate cell death. *Nat. Rev. Mol. Cell Biol.* 9: 47–59.
- Deng, J., N. Carlson, K. Takeyama, P. Dal Cin, M. Shipp, and A. Letai. 2007. BH3 profiling identifies three distinct classes of apoptotic blocks to predict response to ABT-737 and conventional chemotherapeutic agents. *Cancer Cell* 12: 171–185.
- Wei, M. C., W. X. Zong, E. H. Cheng, T. Lindsten, V. Panoutsakopoulou, A. J. Ross, K. A. Roth, G. R. MacGregor, C. B. Thompson, and S. J. Korsmeyer. 2001. Proapoptotic BAX and BAK: a requisite gateway to mitochondrial dysfunction and death. *Science* 292: 727–730.
- Lessene, G., P. E. Czabotar, B. E. Sleebs, K. Zobel, K. N. Lowes, J. M. Adams, J. B. Baell, P. M. Colman, K. Deshayes, W. J. Fairbrother, et al. 2013. Structure-guided design of a selective BCL-X_L inhibitor. *Nat. Chem. Biol.* 9: 390–397.
- Leverson, J. D., H. Zhang, J. Chen, S. K. Tahir, D. C. Phillips, J. Xue, P. Nimmer, S. Jin, M. Smith, Y. Xiao, et al. 2015. Potent and selective small-molecule MCL-1 inhibitors demonstrate on-target cancer cell killing activity as single agents and in combination with ABT-263 (navitoclax). *Cell Death Dis.* 6: e1590.
- Kotschy, A., Z. Szlavik, J. Murray, J. Davidson, A. L. Maragno, G. Le Toumelin-Brazzat, M. Chanrion, G. L. Kelly, J. N. Gong, D. M. Moujalled, et al. 2016. The MCL1 inhibitor S63845 is tolerable and effective in diverse cancer models. *Nature* 538: 477–482.
- Foight, G. W., J. A. Ryan, S. V. Gullá, A. Letai, and A. E. Keating. 2014. Designed BH3 peptides with high affinity and specificity for targeting Mcl-1 in cells. *ACS Chem. Biol.* 9: 1962–1968.
- Nikitin, P. A., A. M. Price, K. McFadden, C. M. Yan, and M. A. Luftig. 2014. Mitogen-induced B-cell proliferation activates Chk2-dependent G1/S cell cycle arrest. *PLoS One* 9: e87299.
- Hawkins, E. D., M. L. Turner, M. R. Dowling, C. van Gend, and P. D. Hodgkin. 2007. A model of immune regulation as a consequence of randomized lymphocyte division and death times. *Proc. Natl. Acad. Sci. USA* 104: 5032–5037.

23. Thomas, L. W., C. Lam, R. E. Clark, M. R. White, D. G. Spiller, R. J. Moots, and S. W. Edwards. 2012. Serine 162, an essential residue for the mitochondrial localization, stability and anti-apoptotic function of Mcl-1. *PLoS One* 7: e45088.
24. Inuzuka, H., S. Shaik, I. Onoyama, D. Gao, A. Tseng, R. S. Maser, B. Zhai, L. Wan, A. Gutierrez, A. W. Lau, et al. 2011. SCF^{F^{bw7}} regulates cellular apoptosis by targeting MCL1 for ubiquitylation and destruction. *Nature* 471: 104–109.
25. Néron, S., G. Suck, X. Z. Ma, D. Sakac, A. Roy, Y. Katsman, N. Dussault, C. Racine, and D. R. Branch. 2006. B cell proliferation following CD40 stimulation results in the expression and activation of Src protein tyrosine kinase. *Int. Immunol.* 18: 375–387.
26. Donahue, A. C., and D. A. Fruman. 2003. Proliferation and survival of activated B cells requires sustained antigen receptor engagement and phosphoinositide 3-kinase activation. *J. Immunol.* 170: 5851–5860.
27. Huggins, J., T. Pellegrin, R. E. Felgar, C. Wei, M. Brown, B. Zheng, E. C. Milner, S. H. Bernstein, I. Sanz, and M. S. Zand. 2007. CpG DNA activation and plasma-cell differentiation of CD27⁺ naive human B cells. *Blood* 109: 1611–1619.
28. Jourdan, M., A. Caraux, J. De Vos, G. Fiol, M. Larroque, C. Cognot, C. Bret, C. Duperray, D. Hose, and B. Klein. 2009. An in vitro model of differentiation of memory B cells into plasmablasts and plasma cells including detailed phenotypic and molecular characterization. *Blood* 114: 5173–5181.
29. Chou, T. C. 2010. Drug combination studies and their synergy quantification using the Chou-Talalay method. *Cancer Res.* 70: 440–446.
30. Peperzak, V., I. Vikström, J. Walker, S. P. Glaser, M. LePage, C. M. Coquery, L. D. Erickson, K. Fairfax, F. Mackay, A. Strasser, et al. 2013. Mcl-1 is essential for the survival of plasma cells. *Nat. Immunol.* 14: 290–297.
31. Sarosiek, K. A., C. Fraser, N. Muthalagu, P. D. Bholra, W. Chang, S. K. McBrayer, A. Cantlon, S. Fisch, G. Golomb-Mello, J. A. Ryan, et al. 2017. Developmental regulation of mitochondrial apoptosis by c-Myc governs age- and tissue-specific sensitivity to cancer therapeutics. *Cancer Cell* 31: 142–156.
32. Ryan, J., and A. Letai. 2013. BH3 profiling in whole cells by fluorimeter or FACS. *Methods* 61: 156–164.
33. Gaudette, B. T., N. N. Iwakoshi, and L. H. Boise. 2014. Bcl-x_L protein protects from C/EBP homologous protein (CHOP)-dependent apoptosis during plasma cell differentiation. *J. Biol. Chem.* 289: 23629–23640.
34. Wheeler, M. L., and A. L. Defranco. 2012. Prolonged production of reactive oxygen species in response to B cell receptor stimulation promotes B cell activation and proliferation. *J. Immunol.* 189: 4405–4416.
35. Jellusova, J., M. H. Cato, J. R. Appgar, P. Ramezani-Rad, C. R. Leung, C. Chen, A. D. Richardson, E. M. Conner, R. J. Benschop, J. R. Woodgett, and R. C. Rickert. 2017. Gsk3 is a metabolic checkpoint regulator in B cells. *Nat. Immunol.* 18: 303–312.
36. Ranuncolo, S. M., J. M. Polo, J. Dierov, M. Singer, T. Kuo, J. Grealley, R. Green, M. Carroll, and A. Melnick. 2007. Bcl-6 mediates the germinal center B cell phenotype and lymphomagenesis through transcriptional repression of the DNA-damage sensor ATR. *Nat. Immunol.* 8: 705–714.
37. Nikitin, P. A., C. M. Yan, E. Forte, A. Bocedi, J. P. Tourigny, R. E. White, M. J. Allday, A. Patel, S. S. Dave, W. Kim, et al. 2010. An ATM/Chk2-mediated DNA damage-responsive signaling pathway suppresses Epstein-Barr virus transformation of primary human B cells. *Cell Host Microbe* 8: 510–522.
38. Price, A. M., J. Dai, Q. Bazot, L. Patel, P. A. Nikitin, R. Djavadian, P. S. Winter, C. A. Salinas, A. P. Barry, K. C. Wood, et al. 2017. Epstein-Barr virus ensures B cell survival by uniquely modulating apoptosis at early and late times after infection. *Elife* 6: e22509.
39. Tsujimoto, Y., J. Cossman, E. Jaffe, and C. M. Croce. 1985. Involvement of the bcl-2 gene in human follicular lymphoma. *Science* 228: 1440–1443.
40. Kridel, R., L. H. Sehn, and R. D. Gascoyne. 2012. Pathogenesis of follicular lymphoma. *J. Clin. Invest.* 122: 3424–3431.
41. Wenzel, S. S., M. Grau, C. Mavis, S. Hailfinger, A. Wolf, H. Madle, G. Deeb, B. Dörken, M. Thome, P. Lenz, et al. 2013. MCL1 is deregulated in subgroups of diffuse large B-cell lymphoma. *Leukemia* 27: 1381–1390.
42. Klein, U., G. Klein, B. Ehlin-Henriksson, K. Rajewsky, and R. Küppers. 1995. Burkitt's lymphoma is a malignancy of mature B cells expressing somatically mutated V region genes. *Mol. Med.* 1: 495–505.
43. Dave, S. S., K. Fu, G. W. Wright, L. T. Lam, P. Kluin, E. J. Boerma, T. C. Greiner, D. D. Weisenburger, A. Rosenwald, G. Ott, et al; Lymphoma/Leukemia Molecular Profiling Project. 2006. Molecular diagnosis of Burkitt's lymphoma. *N. Engl. J. Med.* 354: 2431–2442.
44. Kelly, G. L., S. Grabow, S. P. Glaser, L. Fitzsimmons, B. J. Aubrey, T. Okamoto, L. J. Valente, M. Robati, L. Tai, W. D. Fairlie, et al. 2014. Targeting of MCL-1 kills MYC-driven mouse and human lymphomas even when they bear mutations in p53. *Genes Dev.* 28: 58–70.
45. Gupta, V. A., S. M. Matulis, J. E. Conage-Pough, A. K. Nooka, J. L. Kaufman, S. Lonial, and L. H. Boise. 2017. Bone marrow microenvironment-derived signals induce Mcl-1 dependence in multiple myeloma. *Blood* 129: 1969–1979.
46. Wuillème-Toumi, S., N. Robillard, P. Gomez, P. Moreau, S. Le Guillou, H. Avet-Loiseau, J. L. Harousseau, M. Amiot, and R. Bataille. 2005. Mcl-1 is overexpressed in multiple myeloma and associated with relapse and shorter survival. *Leukemia* 19: 1248–1252.
47. Morales, A. A., M. Kurtoglu, S. M. Matulis, J. Liu, D. Siefker, D. M. Gutman, J. L. Kaufman, K. P. Lee, S. Lonial, and L. H. Boise. 2011. Distribution of Bim determines Mcl-1 dependence or codependence with Bcl-x_L/Bcl-2 in Mcl-1-expressing myeloma cells. *Blood* 118: 1329–1339.